Seasonal variation of methane, water vapor, and nitrogen oxides near the tropopause: Satellite observations and model simulations

Mijeong Park
School of Earth and Environmental Sciences, Seoul National University, Seoul, Korea

William J. Randel, Douglas E. Kinnison, and Rolando R. Garcia
National Center for Atmospheric Research, Boulder, Colorado, USA

Wookap Choi
School of Earth and Environmental Sciences, Seoul National University, Seoul, Korea

Received 21 April 2003; revised 19 November 2003; accepted 3 December 2003; published 5 February 2004.

[1] Seasonal variations of several trace constituents near the tropopause are analyzed based on satellite measurements, and results are compared to a recent numerical model simulation. We examine methane, water vapor, and nitrogen oxides (NO_x) derived from Halogen Occultation Experiment (HALOE) satellite observations; these species have strong gradients near the tropopause, so that their seasonality is indicative of stratosphere-troposphere exchange (STE) and circulation in the near-tropopause region. Model results are from the Model for Ozone and Related Chemical Tracers (MOZART) stratosphere-troposphere chemical transport model (CTM). Results show overall good agreement between observations and model simulations for methane and water vapor, whereas nitrogen oxides near the tropopause are much lower in the model than suggested by HALOE data. The latter difference is probably related to the lightning and convective parameterizations incorporated in MOZART, which produce NO_x maxima not near the tropopause, but in the upper troposphere. Constituent seasonal variations highlight the imporatance of the Northern Hemisphere (NH) summer monsoons as regions for transport into the lowermost stratosphere. In MOZART, there is clear evidence that air from the monsoon region is transported into the tropics and entrained into the upward Brewer-Dobson circulation, bypassing the tropical tropopause. *INDEX TERMS:* 0341 Atmospheric Composition and Structure: Middle atmosphere—constituent transport and chemistry (3334); 0368 Atmospheric Composition and Structure: Troposphere—constituent transport and chemistry; 3334 Meteorology and Atmospheric Dynamics: Middle atmosphere dynamics (0341, 0342); 3362 Meteorology and Atmospheric Dynamics: Stratosphere/troposphere interactions; *KEYWORDS:* Stratosphere, tropopause, methane, water, reactive nitrogen

Citation: Park, M., W. J. Randel, D. E. Kinnison, R. R. Garcia, and W. Choi (2004), Seasonal variation of methane, water vapor, and nitrogen oxides near the tropopause: Satellite observations and model simulations, *J. Geophys. Res.*, *109*, D03302, doi:10.1029/2003JD003706.

1. Introduction

[2] The range of altitudes surrounding the tropopause has received considerable attention because of the importance of the dynamical, radiative, and chemical processes that take place therein. This near tropopause region may be considered to encompass the upper troposphere, as well as the lowermost stratosphere discussed by *Holton et al.* [1995], and is often referred to as the upper troposphere/lower stratosphere (UTLS). In the lower stratosphere, transport is influenced by the mean meridional (or Brewer-Dobson) circulation, driven by planetary Rossby waves that dissipate in the stratosphere, plus quasi-isentropic horizontal mixing. In the midlatitude upper troposphere, synoptic-scale Rossby waves play important roles in vertical transport and in quasi-isentropic mixing along the subtropical tropopause gaps. In the tropics, the tropopause region is influenced by the upward Brewer-Dobson circulation, and by tropospheric processes ranging from rapid vertical transport by convective mixing to the large-scale cells excited by convective heat release (the Walker and Hadley cells, and the summer monsoons).

[3] Chemically, the tropopause region is important because stratospheric trace gas distributions depend on the interplay between dynamics and chemistry taking place near the tropopause. Air reaching the lower stratosphere in the tropics is entrained into the Brewer-Dobson circulation and

0148-0227/04/2003JD003706$09.00

distributed throughout the middle atmosphere. Compounds of tropospheric origin such as methane, nitrous oxide, chlorofluorocarbons (CFCs), and water vapor are the source gases for the principal chemical families (NO_x, ClO_x, and HO_x) that control the abundance of ozone in the stratosphere and above. The distribution of these families in the lower stratosphere is determined by the interaction among transport, photochemistry and microphysical processes. For example, NO_x can enter the lower stratosphere as nitric oxide produced by lightning in deep convective systems; water vapor mixing ratios are extremely sensitive to tropical tropopause temperatures, where the cold-trap effect dehydrates air entering the stratosphere; and at high latitudes in winter, water vapor and NO_x compounds take part in heterogeneous chemical reactions that can activate chlorine and thus control the destruction of ozone. Ozone and water vapor absorb and emit radiation in the infrared, and ozone also absorbs shortwave solar radiation; the presence of ozone and water vapor makes the tropopause region important for the radiative budget of both the troposphere and lower stratosphere [*Houghton et al.*, 2001].

[4] For all of these reasons, it is important that comprehensive numerical models be able to simulate the tropopause region realistically if the models are to be used to predict the response of the global atmosphere to, for example, changes in gases such as CO_2, methane and CFCs. Model calculations can be compared to in-situ observations (e.g., aircraft measurements, ozonesondes, etc.), but a thorough evaluation of General Circulation Model (GCM) performance must include comparisons of global-scale variability as derived from satellite observations.

[5] The HALOE instrument, onboard the Upper Atmosphere Research Satellite (UARS) spacecraft, has been making measurements of temperature, water vapor (H_2O), methane (CH_4), ozone (O_3), nitric oxide (NO), nitrogen dioxide (NO_2), and the halogen species (HF and HCl) from December 1991 to date [*Russell et al.*, 1993]. These data have been used to study climatological variability in numerous studies [e.g., *Rosenlof et al.*, 1997; *Jackson et al.*, 1998; *Randel et al.*, 1998, 2001; *Beaver and Russell*, 1998]. HALOE provides nearly continuous coverage outside of the polar caps at altitudes that, in principle, can include the tropopause region, although the lower limit of observation is limited by loss of signal (dependent on the specific channel), and by the presence of clouds. HALOE data has been used in many studies of stratospheric and mesospheric chemistry and transport, but its use in the tropopause region has been more limited, especially for NO_x species.

[6] The purpose of this paper is to compare simulations of near-tropopause chemistry obtained from MOZART with HALOE observations. The MOZART calculations are driven by dynamical fields calculated with the Whole Atmosphere Community Climate Model (WACCM), a comprehensive GCM that spans both the troposphere and middle atmosphere, with moderately high vertical resolution ($\sim$1.5 km) in the upper troposphere and lower stratosphere. By studying the large-scale seasonal variations in the model and the observations we attempt to shed light on the validity of both, and on the physical and chemical processes that operate in the tropopause region. In particular, we emphasize the role of tropical deep convection in vertical transport of tropospheric source gases; the large-scale transport by organized circulations, such as the monsoon systems, that are forced by latent heat release in sub-tropical convection; and the interaction between convection and large-scale motion in producing dehydration of air that enters the stratosphere.

[7] We note that the comparisons here focus on the large-scale seasonal cycle and not on synoptic timescales, so that we are not explicitly disgnosing stratosphere-troposphere exchange (STE) in any detail. However, the presence of seasonally varying structures with spatial coherence between the middle/upper troposphere and lower stratosphere is strong circumstantial evidence for STE. For the model we can examine the entire stratosphere-troposphere region, whereas the satellite data only extend down to the near tropopause level. On the basis of similar space-time variability near the tropopause, we then infer some conclusions about processes in the real atmosphere. Future studies will focus on details of synoptic variability near the tropopause in the model, and processes that contribute to STE.

[8] In sections 2 and 3, respectively, we describe the HALOE observations and the WACCM and MOZART models used in these comparisons. The remainder of the paper is devoted to detailed comparisons of methane, water vapor and oxides of nitrogen. We show that there is broad agreement in observed and calculated space-time distributions of methane and water vapor, but some substantial differences for nitrogen oxides fields. We also compared ozone in the tropopause region, and found good agreement between HALOE and MOZART (results are not included here). The comparisons here are aimed at exploring the usefulness of HALOE data in the UTLS, and point to some interesting transport mechanisms that merit further investigation.

2. Observational Data and Model Details

2.1. HALOE Satellite Data

[9] The HALOE provides high quality vertical profiles of CH_4, H_2O, NO, and NO_2 using solar occultation measurements [*Russell et al.*, 1993]. CH_4 and NO are measured by a gas filter correlation technique, while H_2O and NO_2 are measured by wide band radiometry, which is a direct measurement of the energy absorbed during occultation. The HALOE measurements cover the middle atmosphere (with upper limit of observation depending on species), and the retrievals extend downward to near the tropopause or into the upper troposphere, being cut off in the presence of opaque clouds. These HALOE solar occultation measurements are characterized by high accuracy and relatively high vertical resolution ($\sim$2 km).

[10] Error characteristics for the HALOE data in the lower stratosphere and tropopause region are as follows. The total error for individual methane profiles including systematic and random uncertainties is 20% for the 50–100 hPa region [*Park et al.*, 1996]. The estimated error budget for water vapor in this height range is $\pm$10–15% [*Harries et al.*, 1996], and detailed intercomparisons in the *Stratospheric Processes and Their Role in Climate* (*SPARC*) [2000] water vapor assessment suggest HALOE data have a dry bias of $\sim$10% compared to other measure-

ments over ~60–100 hPa. The estimated errors of nitric oxide and nitrogen dioxide are discussed by *Gordley et al.* [1996]. The retrieval uncertainties increase rapidly below ~25 km (to over 50%), due to smaller weaker signals and systematic uncertainties (such as pressure registration and interfering species). The few available correlative comparisons in *Gordley et al.* [1996] suggest NO_2 may be biased low below 25 km by up to 0.5 ppbv (with too few comparisons to comment on NO). Overall the HALOE NO and NO_2 data near the tropopause have received less attention than data above 25 km, and should be treated cautiously. Indeed, part of the motivation of this study is to evaluate the utility and geophysical consistency of these data at the lowest retrieved altitudes.

[11] The HALOE solar occultation sampling provides 15 sunrise and 15 sunset measurements per day, each near the same latitude but spaced ~24 degrees apart in longitude. The latitude sampling progresses in time so that much of the latitude range 60°N–S is sampled in one month. Here we use version 19 HALOE data in level 2 format for the period from October 1992 to September 2002. The period prior to October 1992 is not included here because of enhanced retrieval errors due to Pinatubo aerosols [*Hervig et al.*, 1995]. For the analyses presented here, only profiles with error uncertainties >100% were included. We also omit methane profiles where the mixing ratio exceeds 2.0 ppmv, which is larger than maximum tropospheric values [e.g., *Dlugokencky et al.*, 1998] (this results in only a 2% loss of available profiles). Gridded maps of HALOE data (on a 5° longitude by 5° latitude grid) are constructed on standard log-pressure levels using Delaunay triangulation [*Schroeder and Shepherd*, 1988]. Monthly means for the 1992–2002 periods are constructed, and the monthly means are averaged to create 10-year averaged climatology. Sunrise and sunset measurements are combined for CH_4 and H_2O data, whereas they are treated separately for NO and NO_2 (as discussed in Section 3.4 below).

[12] Meteorological fields displayed with the HALOE data are derived from the National Centers for Environmental Prediction (NCEP)/NCAR reanalysis [*Kalnay et al.*, 1996]. These include (potential) temperature and tropopause height, the latter derived using the thermal lapse rate criterion, as obtained directly from the NCEP/NCAR output.

2.2. Model Description

2.2.1. Climate Model

[13] The WACCM, Version 1b (WACCM1b), is a comprehensive dynamical model, spanning the range of altitude from the Earth's surface to the thermosphere. This model is built upon the numerical framework of the NCAR Community Climate System Model (CCSM), and is envisaged as a flexible model environment, whose domain and component modules can be configured according to the specific problem under study (http://acd.ucar.edu/models/WACCM).

[14] The dynamical framework of Whole Atmosphere Community Climate Model (WACCM) is derived from the Middle Atmosphere Community Climate Model (MACCM), which is in turn based on the standard NCAR Community Climate Model (CCM). MACCM and its climatology are described in detail in *Boville* [1995] and *Kiehl et al.* [1998]. The dynamical governing equations are solved with a semi-Lagrangian technique [*Williamson and Olson*, 1994] at T63 horizontal resolution. For this study, WACCM1b was integrated from 1979 to 2001 using observed sea surface temperatures and green-house gas abundances. Meteorological outputs from this simulation were used to "drive" a the MOZART 3-D CTM, as discussed below.

2.2.2. Chemical Transport Model

[15] The Model for Ozone and Related chemical Tracers (MOZART) is a 3-D global CTM that can be run using observed winds or wind fields derived from a GCM [*Brasseur et al.*, 1998; *Hauglustaine et al.*, 1998; *Horowitz et al.*, 2004]. (http://acd.ucar.edu/models/MOZART). The model horizontal and vertical resolution is determined by that of the meteorological fields, which. In in this study the horizontal resolution is a 2.8 longitude by 2.8 latitude grid. The vertical extentmodel domain is divided vertically into 66 hybrid sigma-pressure levels, extending from the surface to ~140 km. The vertical resolution is ~1.0–1.2 km near the tropopause, and ~1.5 km in the stratosphere. MOZART is driven by global wind, temperature, and cloud fields provided every 3 hours from archived WACCM1b results.

[16] MOZART, version 3 (MOZART-3), used in this study, was developed to represent chemical and physical processes from the surface through the thermosphere. In this study, MOZART-3 adopted a chemical scheme representative of chemical and physical processes of the stratosphere. This The MOZART chemical mechanism includes 48 chemical species and ~120 chemical and photochemical reactions. Source gas surface boundary conditions are trended based on historical observations from 1979 through 2001 [*Garcia and Solomon*, 1994], using the values published by the Intergovernmental Panel on Climate Change (IPCC) reports [*Houghton et al.*, 1996, 2001]. The simulation includes a surface flux boundary condition for CH_4, with the surface volume mixing ratio scaled to follow the historical trend of CH_4 between 1979 and 2001. The model accounts for surface emissions of NO_x and CO based on the emission inventories as described by *Horowitz et al.* [2004]. NO_x source from lightning is distributed according to the location of convective clouds based on *Price et al.* [1997] with a "C-shaped" vertical profile following *Pickering et al.* [1998]. Aircraft emissions of NO_x and CO are included in the model, based on *Friedl* [1997]. Advective transport incorporates the flux form semi-Lagrangian transport algorithm of *Lin and Rood* [1996]. The hydrological cycle follows the approach discussed in *Rasch and Kristjansson* [1998].

[17] For comparisons with observations, monthly averages of CH_4, H_2O, NO, and NO_2 abundances were taken from a 5-year sample of a long-term integration. For reference, cross sections of MOZART results include isentropic and tropopause height derived from the WACCM1b meteorological fields; the tropopause height is defined by the lapse rate criterion. Model-observed comparisons of CH4 and NOx are made on pressure surfaces near the tropospause, because this is the native coordinate for the HALOE retrievals. Results on isentropic levels are very similar. Isentropic level results are included

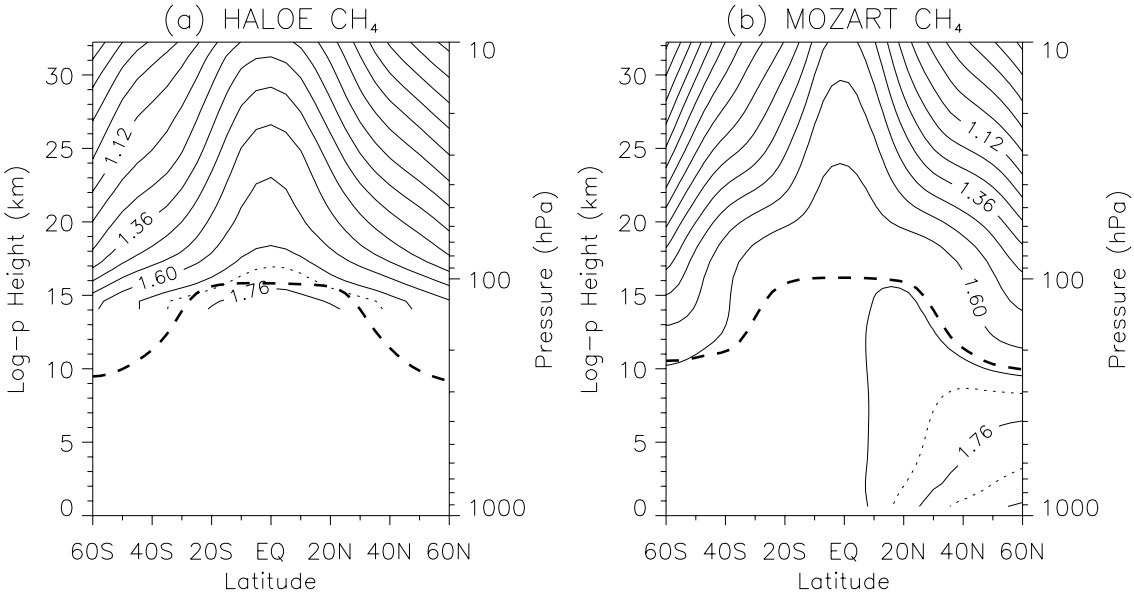

Figure 1. Latitude-altitude cross sections of time averaged zonal mean methane mixing ratio obtained from the (a) HALOE and (b) MOZART. Thick dashed lines denote the respective tropopause for each data set, derived as discussed in the text. Contour interval is 0.08 ppmv, and dashed contours are one half.

for H2O, because the observed seasonal cycle in H2O follows isentropes in the UTLS [*Randel et al.*, 2001].

3. Observed and Modeled Seasonal Variability Near the Tropopause

3.1. Methane

[18] Important information on the transport of mass within the stratosphere, and between the troposphere and stratosphere, has been derived from satellite observations of methane [e.g., *Jones and Pyle*, 1984; *Holton and Choi*, 1988; *Schoeberl et al.*, 1995; *Randel et al.*, 1998]. Methane is produced by biotic activity near the Earth's surface, transported into the stratosphere, and chemically destroyed (oxidized) above 35 km. The photochemical lifetime of CH_4 below 40 km is >100 days, so that the distribution in the stratosphere and UTLS region is determined mainly by the circulation. The global budget and secular trends of atmospheric CH_4 have been discussed in *Dlugokencky et al.* [1998] and *Intergovernmental Panel on Climate Change* [2001]; it is noteworthy that long-term variations of tropospheric CH_4 in the past few years have shown only small increases or negative trends [*Simpson et al.*, 2002].

[19] The time-averaged, zonal mean mixing ratios of CH_4 derived from HALOE data and calculated with MOZART are compared in Figure 1. Note that, in this and similar plots that follow, the MOZART results include tropospheric values, while the HALOE retrievals are available only down to the tropopause region. The overall patterns of MOZART CH_4 are similar to the observations shown in Figure 1, displaying a decrease with altitude and latitude in the stratosphere that reflects the "age" of stratospheric air [*Hall et al.*, 1999]. However, the vertical and latitudinal gradients in the lower stratosphere and tropopause region are weaker in the MOZART results than in HALOE data.

[20] Latitude-time variations in observed and modeled zonal average mixing ratio of CH_4 at 136 hPa are shown in Figure 2. The 136 hPa level is at the lower end of the range of available HALOE CH_4 data; this level is below the altitude of the tropopause in the tropics, and above it in midlatitudes. The overall values from HALOE are somewhat higher than those in MOZART, but both show a similar seasonal cycle with a relative maximum during NH summer (June–September), centered over ~10–40°N. This maximum is associated with the NH summer monsoon circulations, and is slightly larger in the MOZART simulation. Note that the seasonal cycle of tropospheric CH_4 is small and near-surface methane has a minimum in NH summer [*Dlugokencky et al.*, 1994], so that the summer maximum near tropopause level reflects increased vertical transport associated with the monsoon circulations (as shown below).

[21] Spatial structure in monthly average CH_4 at 136 hPa during NH summer (July) is shown in Figure 3. Both HALOE and MOZART results show a relative CH_4 maximum over the South Asian monsoon region (more pronounced in MOZART), and a secondary maximum near North America (relatively stronger in HALOE). Seasonal and longitudinal variation of CH_4 mixing ratio at 136 hPa over the monsoon region (10–30°N) is shown in more detail in Figure 4. The evolution of summer maxima over both the South Asian and North American monsoon regions is broadly similar in model and observations, although the South Asian monsoon maximum is relatively larger in MOZART. Overall these comparisons suggest that the summer monsoon CH_4 maxima simulated in MOZART are realistic in their space-time behavior, although their amplitudes may be too large.

[22] A useful feature of the MOZART simulations is that the patterns observed near the tropopause can be examined into and throughout the troposphere. Figure 5 shows a

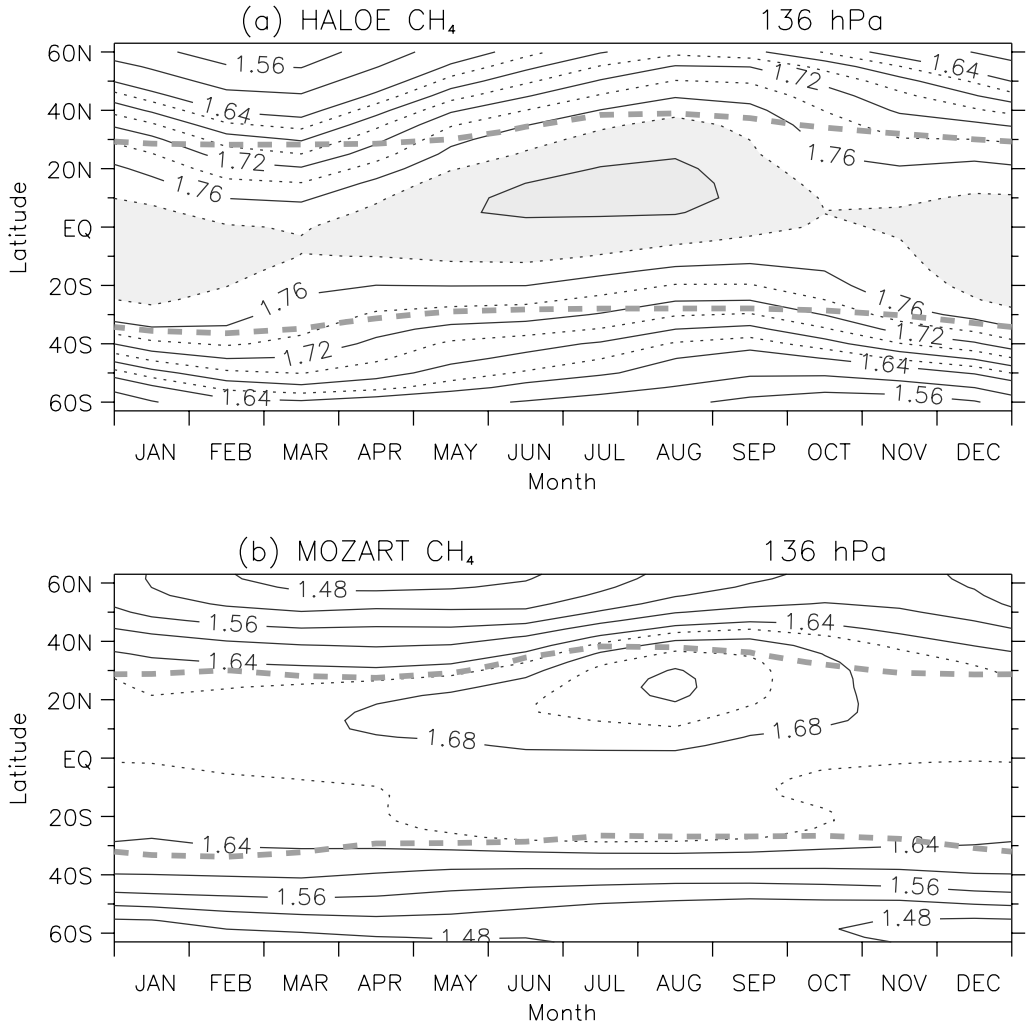

Figure 2. Latitude-time sections of zonal mean methane mixing ratio obtained from (a) HALOE and (b) MOZART at 136 hPa. Full line contour interval is 0.04 ppmv.

meridional cross section of MOZART CH_4 during July, averaged over the South Asian monsoon region (60–120°E). The colors show isopleths of methane in relation to the local tropopause (dashed line) and isentrope structure (solid lines). Relatively high CH_4 values are observed from the surface to the UTLS region at latitudes near 30°N, that in the model is due to transport of (high) surface CH_4 by deep convection in the Asian summer monsoon. Relatively

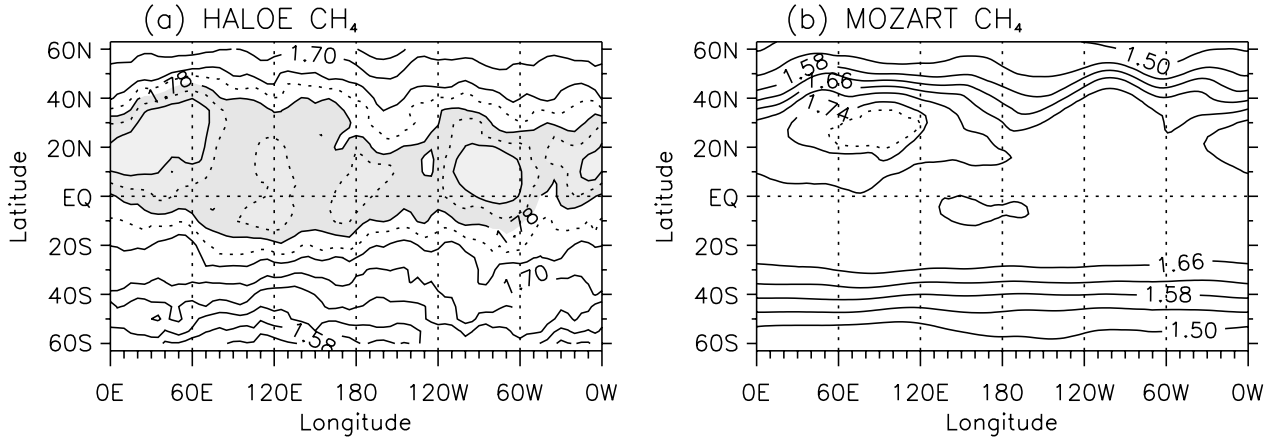

Figure 3. Horizontal structures of methane mixing ratio obtained from (a) HALOE and (b) MOZART at 136 hPa in July. Contour interval is 0.04 ppmv, and values above 1.78 ppmv are shaded.

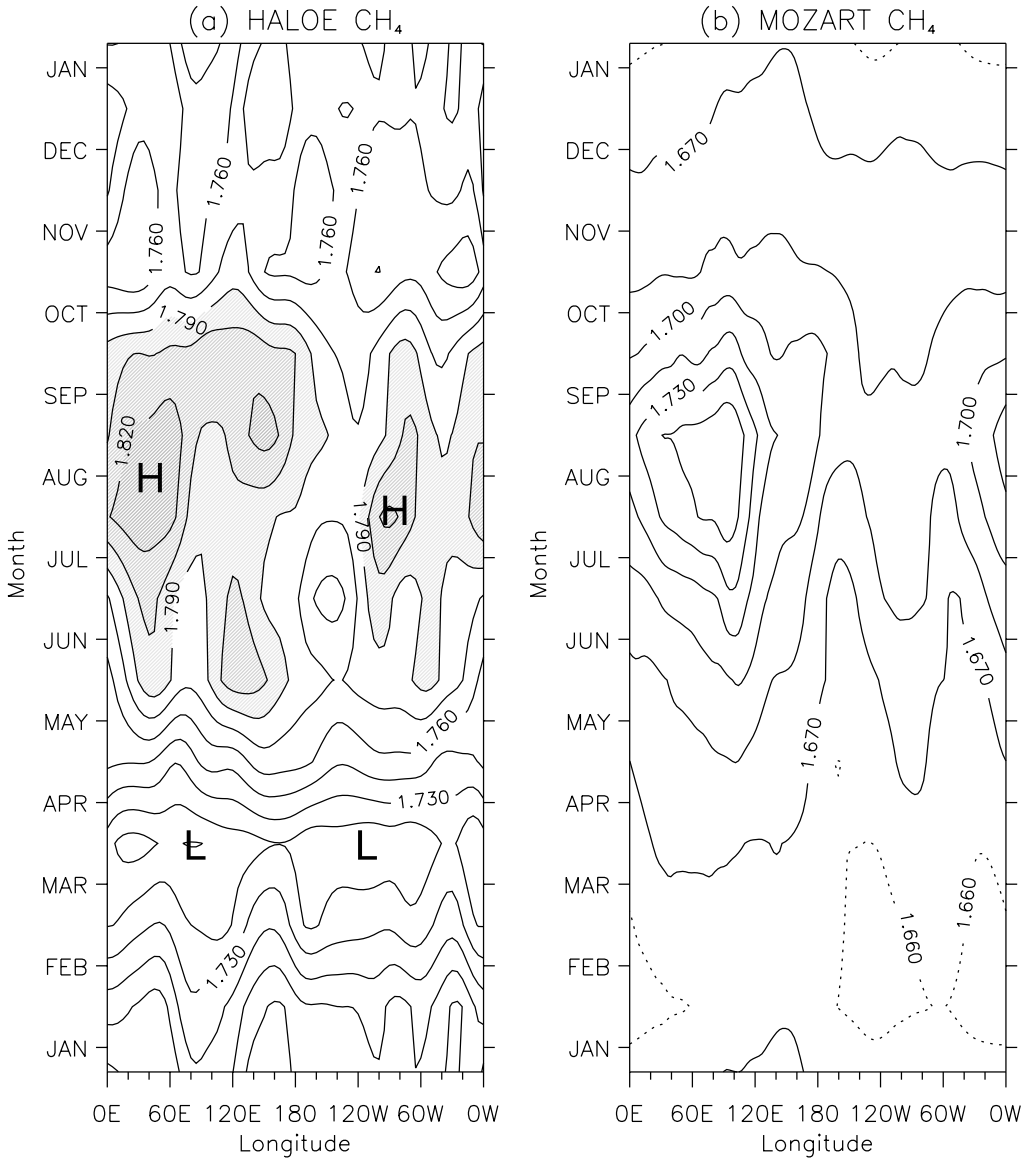

Figure 4. Longitude-time sections of methane mixing ratio of (a) HALOE and (b) MOZART at 136 hPa, averaged between 10° and 30°N. Contour interval is 0.015 ppmv.

high CH_4 is also observed over Northern high latitudes throughout the troposphere. While the local tropopause over the monsoon region is elevated during summer (extending above 100 hPa in the model), it is evident that the high CH_4 values in the upper troposphere extend across the tropopause, directly into the lowermost stratosphere. The sloping isentropes in this region, which cut across the tropopause, provide a relatively uninhibited path for fast meridional transport over a wider range of latitudes. The similarity to HALOE measurements in the UTLS region (Figures 1–4) suggests such a mechanism could facilitate troposphere-stratosphere transport in the real atmosphere as well.

3.2. Water Vapor

[23] Water vapor is an important tracer in the UTLS region because of strong gradients across the tropopause, and simulation of water vapor transport is a stringent test of current global simulations. The water vapor seasonal cycle in the lower stratosphere is set by the annual cycle in tropical tropopause temperatures, and this signal propagates both vertically over the equator (the tropical "tape recorder," *Mote et al.* [1996]) and latitudinally over most of the globe in the lowermost stratosphere [*McCormick et al.*, 1993; *Hintsa et al.*, 1994; *Boering et al.*, 1995; *Rosenlof et al.*, 1997; *Jackson et al.*, 1998; *Randel et al.*, 2001].

[24] Figure 6 shows the altitude-time variation of water vapor over the equator from both HALOE observations and the MOZART simulation (a so-called tape recorder diagram, following *Mote et al.* [1996]). We note that the tropical seasonal cycle of water vapor derived from HALOE at 68 and 56 hPa (19–20 km) is in good agreement with available aircraft measurements and with results derived from the empirical age spectra estimates of *Andrews et al.* [1999]; similar comparisons at 82 hPa suggests that HALOE may underestimate the wet phase during August–October (*Randel et al.* [2001], Figure 9). The dry phase of the

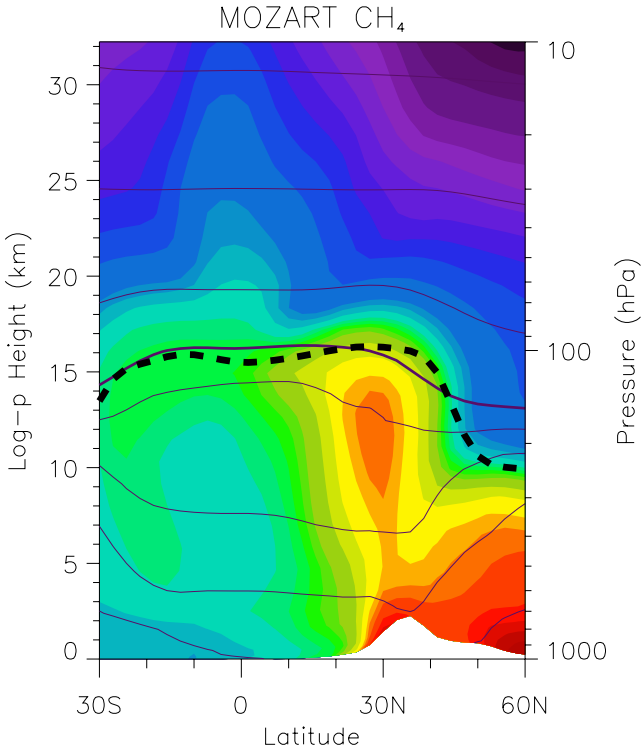

Figure 5. Meridional cross section of MOZART methane mixing ratio in the South Asian monsoon region (60°–120°E) in July. Methane mixing ratio is filled with colors and is not in regular intervals. Thin solid lines denote isentropes of 280, 300, 320, 340, 360, 450, 600, and 800 K (from below), and the dashed line is the thermal tropopause.

MOZART tape recorder in Figure 6 (low water vapor near 100 hPa during NH winter) is quite realistic, occurring with approximately the correct timing and magnitude, and the upward propagation of the dry air is also accurately simulated in the model (implying a realistic upward Brewer-Dobson circulation over the equator). The one outstanding difference from HALOE data occurs during the wet phase, when the model water vapor is substantially higher than HALOE observations.

[25] The cause of the wet bias in MOZART during NH summer is not known, but it is probably not directly related to tropical temperature biases in the underlying WACCM1b simulation. Figure 7 compares the seasonal cycle of tropical 100 hPa temperatures between WACCM1b and European Center for Medium Range Weather Forecasts reanalyses (ERA15). The ERA15 data have realistically cold temperatures near the tropical tropopause, and show good agreement with tropical radiosondes [*SPARC*, 2002]. The WACCM1b-ERA15 comparisons in Figure 7 show reasonable agreement during the cold phase of the annual cycle (NH winter), but show that WACCM1b temperatures are ~2 K too cold during NH summer. This cold bias would result in relatively lower values of lower stratospheric H2O in MOZART (all else being equal), and hence we conclude that tropical temperatures biases are not the cause of the wet biases in MOZART. Similar comparisons over the NH summer monsoon regions show that WACCM1b is also relatively cold compared to analyses.

[26] The latitude-time behavior of water vapor on the 100 hPa isentropic level is compared between HALOE data and the MOZART simulation in Figure 8. An isentropic level is chosen to better illustrate the connection between the tropical seasonal cycle and its extension (transport) to higher latitudes, because the water vapor patterns are

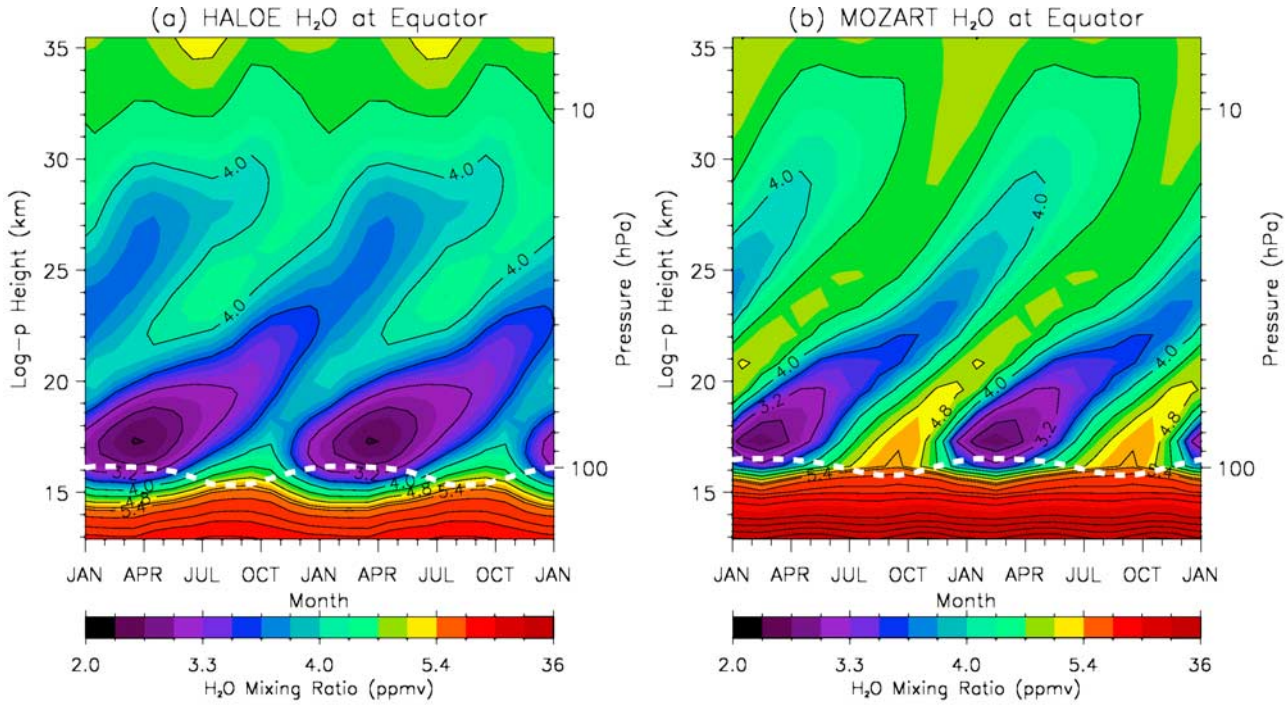

Figure 6. Height-time sections of water vapor mixing ratio over the equator, derived from (a) HALOE observations and (b) MOZART simulation. Two consecutive seasonal cycles are shown in each diagram.

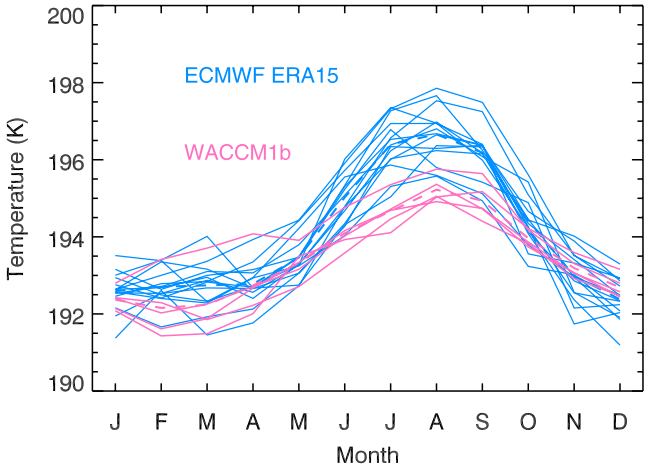

Figure 7. Comparison of the seasonal variation of equatorial 100 hPa temperatures from observations (ERA15 reanalyses, in blue) and WACCM1b simulation (in red). Each line shows the seasonal cycle for one individual year, and the dashed lines are the respective climatologies.

observed to follow the sloping isentropes [*Randel et al.*, 2001]. The HALOE data (Figure 8a) show a strong annual cycle, with a minimum in January–March (associated with coldest tropical temperatures) and maxima during August–October (associated with warm tropical temperatures, plus the summer monsoon circulations centered near 30°N). This diagram shows transport of both the dry and moist phases of the seasonal signal to higher NH latitudes, and into the Southern Hemisphere (SH). Overall the MOZART water vapor (Figure 8b) shows similar behavior, but with the aforementioned wet bias during the NH summer season. While there are differences in detail in the exact timing of extrema, the overall global morphology is reasonably well simulated in MOZART.

[27] The spatial structures of water vapor at 100 hPa during January and July are compared in Figure 9. The NH winter patterns show a relative minimum over the western Pacific in both HALOE and MOZART, and this corresponds to the region of climatological minimum tropopause temperatures (i.e., the "stratospheric fountain" region of *Newell and Gould-Stewart* [1981]). The NH summer water vapor patterns in Figure 9 show reasonable agreement between HALOE and MOZART. Here there are clear

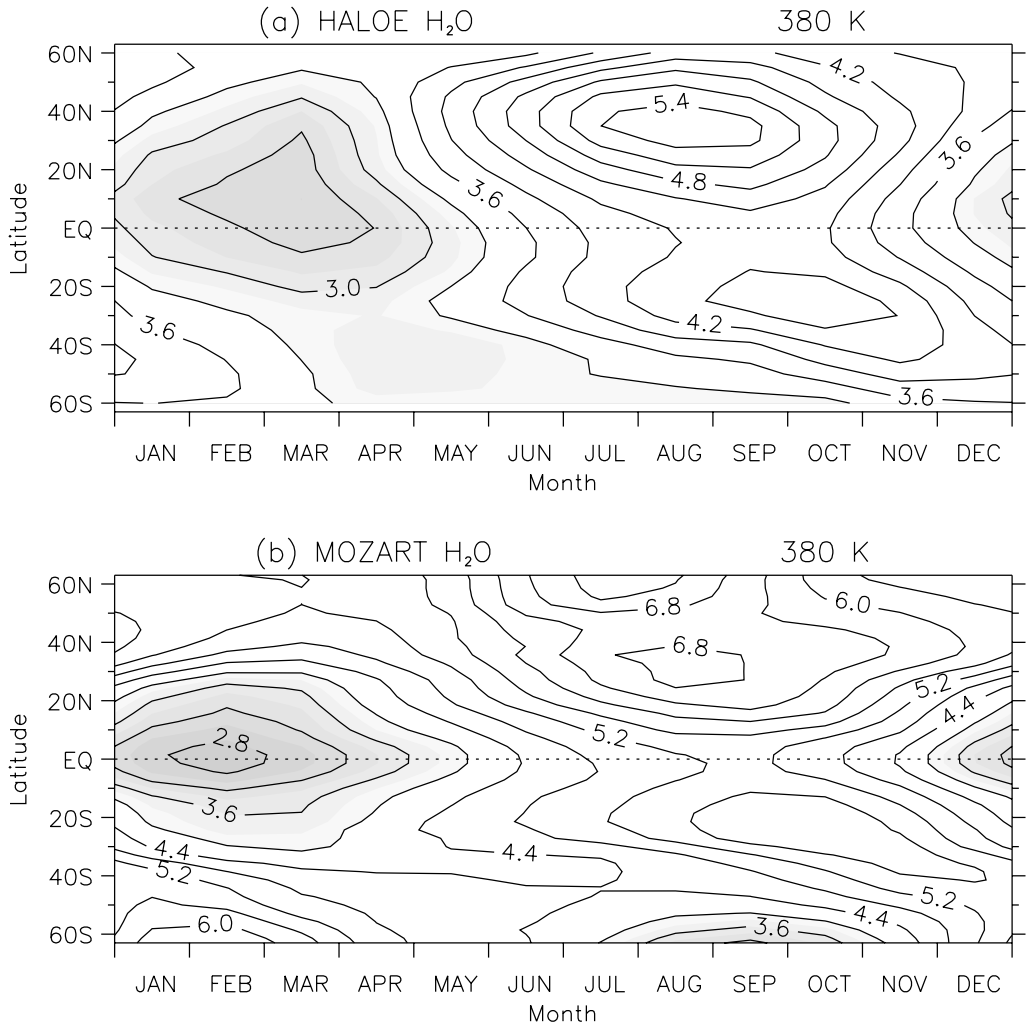

Figure 8. Latitude-time variation of water vapor mixing ratio on the 380 K isentropic surface, derived from (a) HALOE data and (b) MOZART simulation. Contour interval is 0.3 ppmv, and values below 3.3 ppmv are shaded.

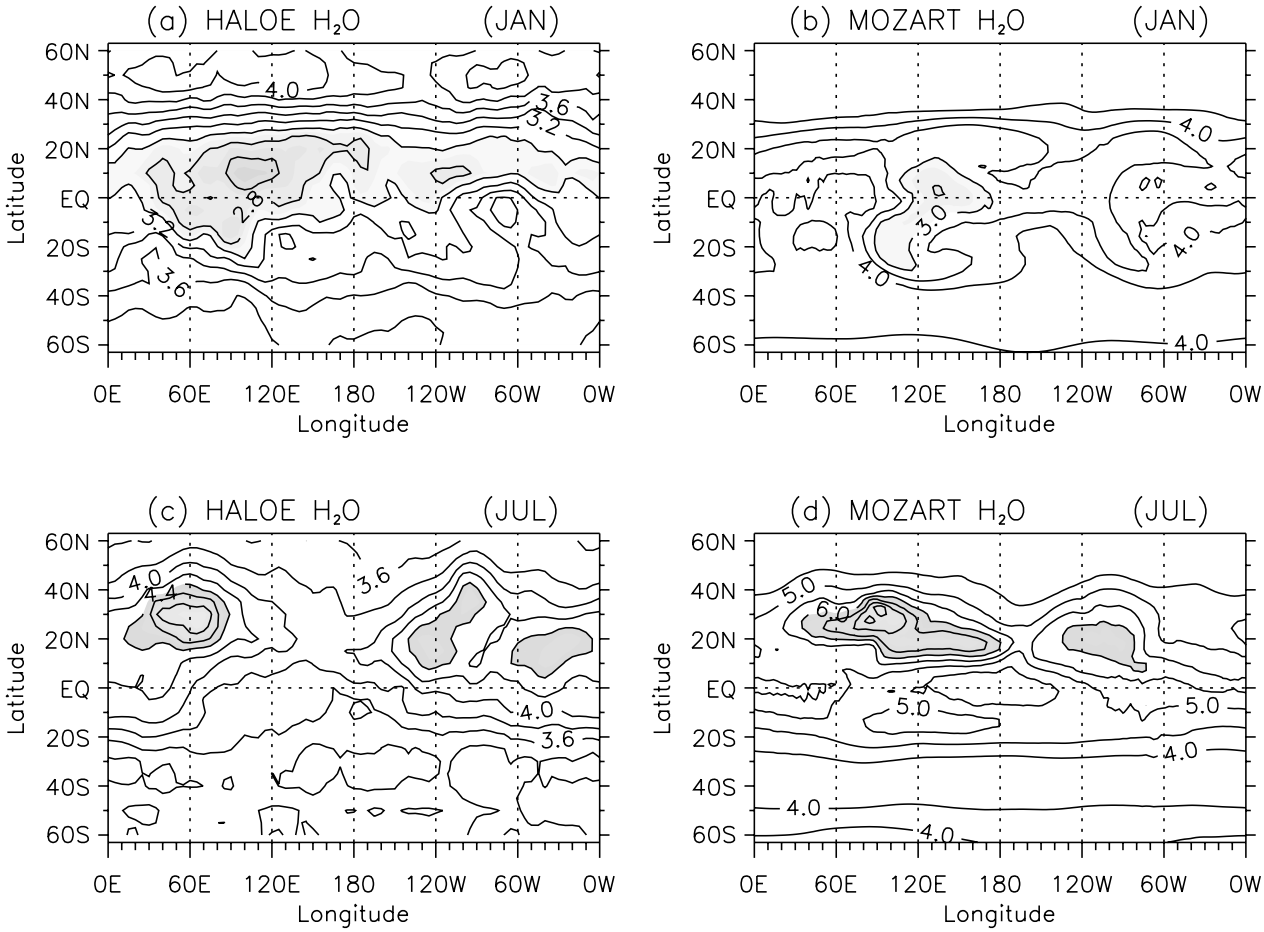

Figure 9. Horizontal structure of water vapor mixing ratio at 100 hPa for (a, c) HALOE and (b, d) MOZART, for January (top) and July (bottom) statistics. Contour interval is 0.2 ppmv for HALOE and 0.5 ppmv for MOZART. Values below 3.0 ppmv are shaded in both January panels, whereas the shaded regions have different (high) values in the July panels.

maxima over the South Asian and North American summer monsoon regions, centered over ~20–40°N (with a somewhat stronger maximum over South Asia). These local maxima are the primary cause of the large NH-SH asymmetry in water vapor seen in Figure 8, and further suggest the importance of the monsoon regions for transport within the UTLS [*Jackson et al.*, 1998; *Dethof et al.*, 1999; *Randel et al.*, 2001].

[28] A cross section of water vapor mixing ratio through the South Asian monsoon region in July is shown in Figure 10, for both HALOE and MOZART data. The MOZART simulation shows an upward bulge of water vapor isopleths in the monsoon region near 30°N, crossing the tropopause and the 380 K isentrope into the lowermost stratosphere. A similar bulge is seen in the July HALOE data, although extension across the climatological tropopause is less evident. In the model the moist monsoon air which enters the lower stratosphere near 30°N is transported both poleward and equatorward, becoming a significant source of moisture on a hemispheric scale. As shown for November data in Figure 11, a remnant of moist air remains in the lower stratosphere after the moistening of upper tropospheric air ceases at the end of summer. In the MOZART simulation this monsoon moist air is transported deep into the tropics by the end of summer, and Figure 11 suggests that the monsoon flow contributes significantly to the moist phase of the tape recorder signal over the equator in the MOZART simulation. Little direct evidence of this is seen in the HALOE data.

3.3. Nitrogen Oxides

[29] Nitrogen oxides play a role in ozone chemistry both in the troposphere and the stratosphere [*Crutzen*, 1970], contributing to ozone formation in the troposphere and ozone destruction in the stratosphere. Major sources of nitrogen oxides are fossil fuel combustion at the surface, biomass burning, soil emission, and lightning [*Seinfeld and Pandis*, 1998; *Pickering et al.*, 1998]. In the upper troposphere, lightning generation of nitrogen oxides, transport from the stratosphere and aircraft emission could be important sources [*Brasseur et al.*, 1996; *Zhang et al.*, 2000].

[30] Nitrogen oxides exhibit a strong diurnal variation; during daylight there are comparable amounts of NO_2 and NO, whereas at night all of the NO is converted to NO_2. The HALOE 100 hPa NO data are consistent with this variability, showing very small values at sunrise and larger values at

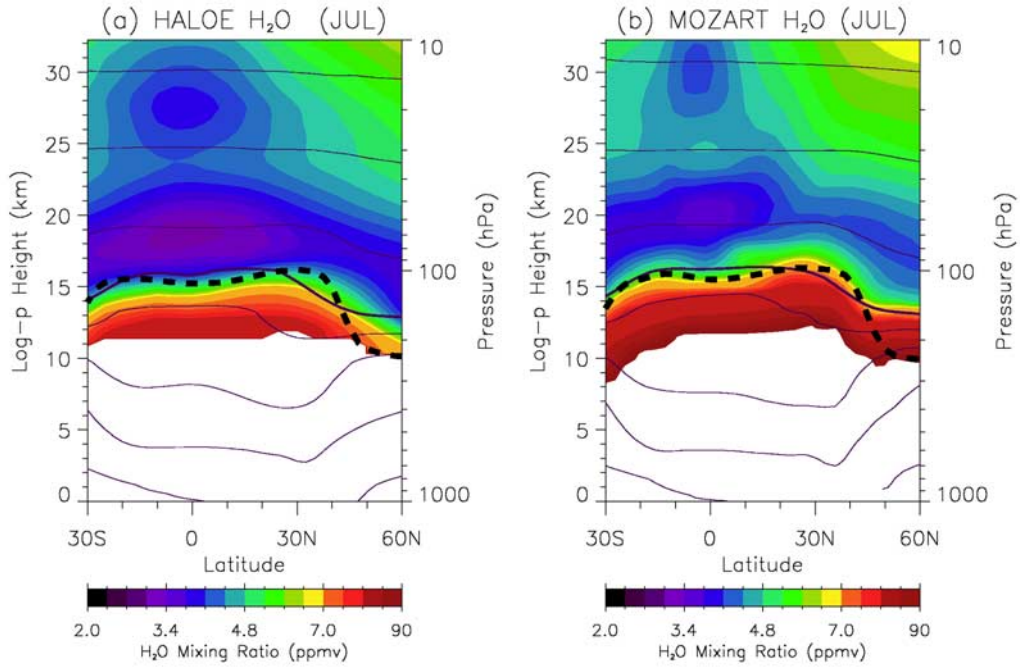

Figure 10. Meridional cross sections of water vapor mixing ratio in the South Asian monsoon region (60°–120°E) in July. Results are shown for (a) HALOE observations and (b) MOZART simulation. The heavy dashed lines indicate the tropopause appropriate for each data set.

sunset. Conversely, the sunrise HALOE NO_2 is larger than sunset values; the combined NO_x (=NO + NO_2) is approximately similar between sunrise and sunset.

[31] The HALOE climatology of sunset NO and NO_2 data at 100 hPa is shown in Figure 12, for statistics in January and July. The NO data show maximum values in low latitudes of ~0.25 ppbv, with spatial maxima in January located near Africa, Indonesia, and South America (i.e., near convection), and July maxima near the South Asian monsoon and (weakly) over North America. The sunset NO_2 data in January show tropical values of similar magnitude, with additional maxima at high summer latitudes (related to the summer NO_x chemistry discussed in *Brühl et al.* [1998]). Larger amplitude (~0.5 ppbv) sunset

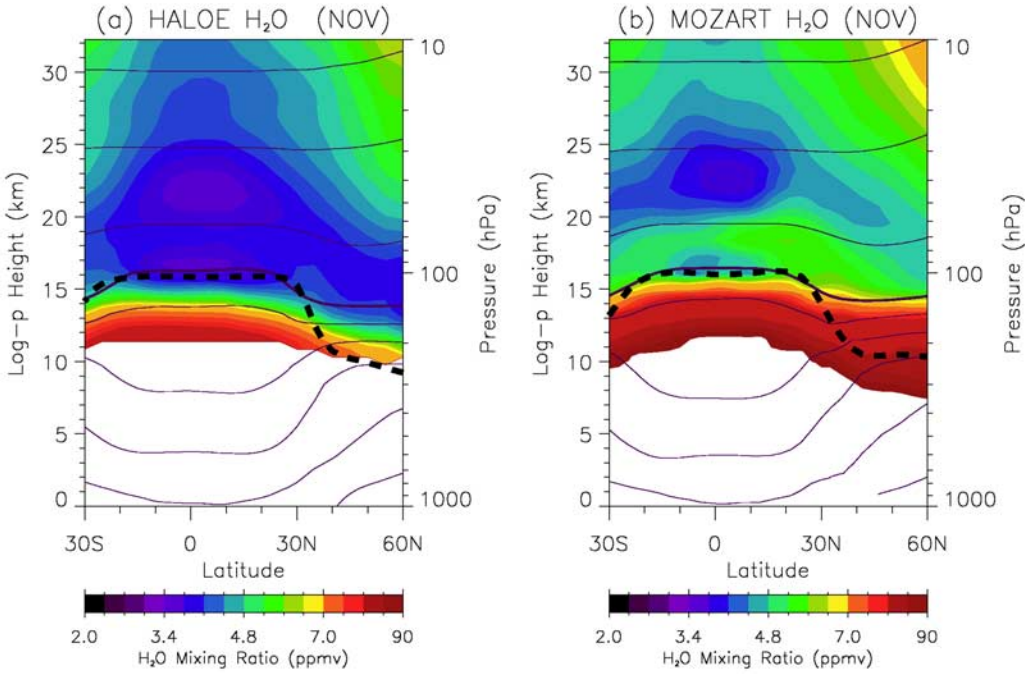

Figure 11. As in Figure 10, but for data during November.

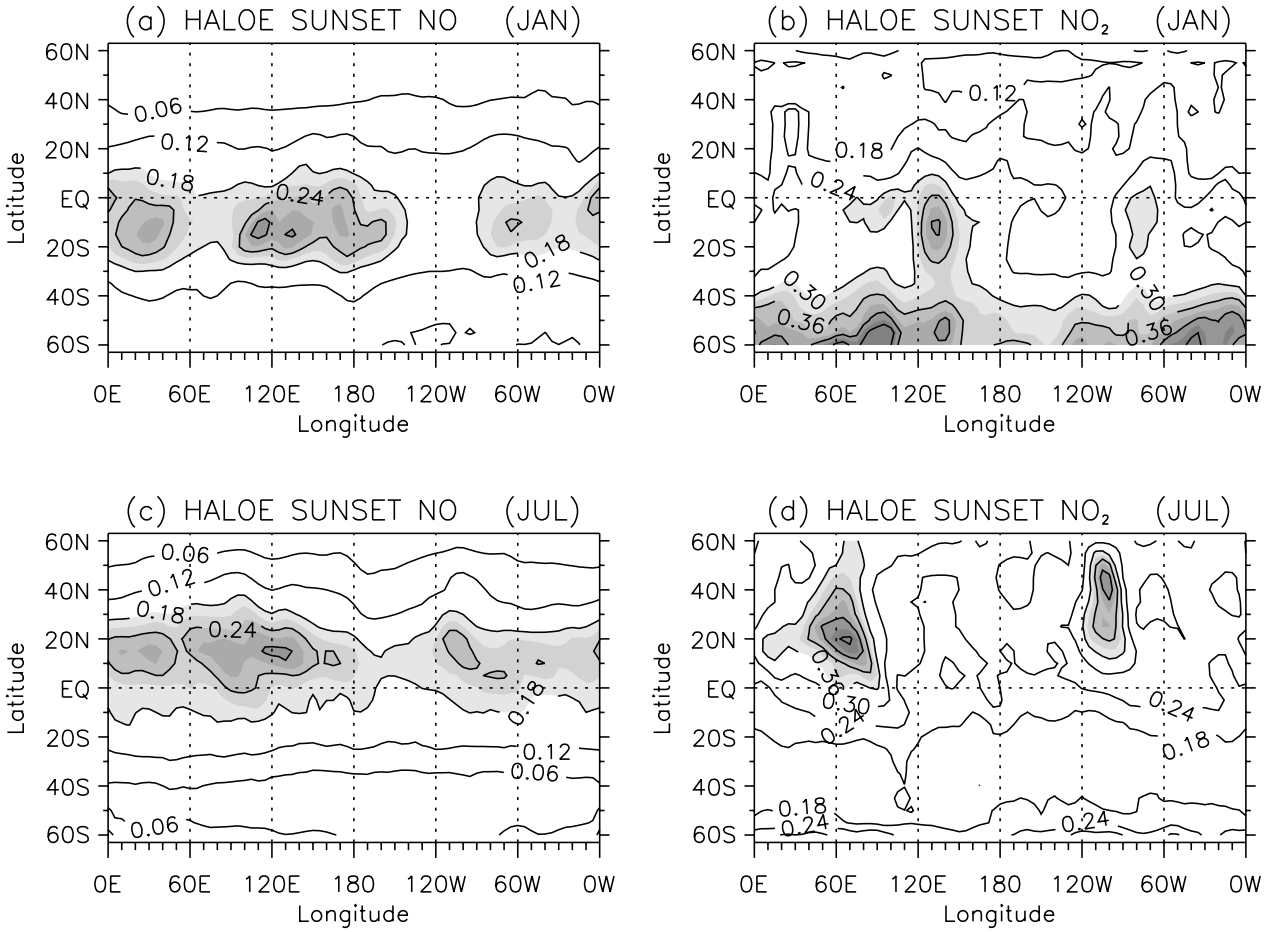

Figure 12. Spatial structure of HALOE sunset climatology for (a, c) NO and (b, d) NO_2, for statistics in January (top) and July (bottom). Contour interval is 0.06 ppmv.

NO_2 maxima are observed in July, centered over Asia and North America; these are somewhat larger than the sunset NO maxima, and are centered at higher summer latitudes.

[32] The combined HALOE sunset NO_x climatology (derived by adding together the individual NO and NO_2 climatologies) is shown in Figure 13 for January and July at 100 hPa. The NO_x data show relative maxima of ~0.5–0.8 ppmv centered over the regions of maximum convection discussed above; similar spatial maxima are observed at 68 hPa, but above this level the NO_x fields become more zonally symmetric. Figure 14 shows the January and July MOZART NO_x results (derived from a full diurnal average) at two pressure levels: 158 hPa and 100 hPa. We show these two levels because there are substantial qualitative differ-

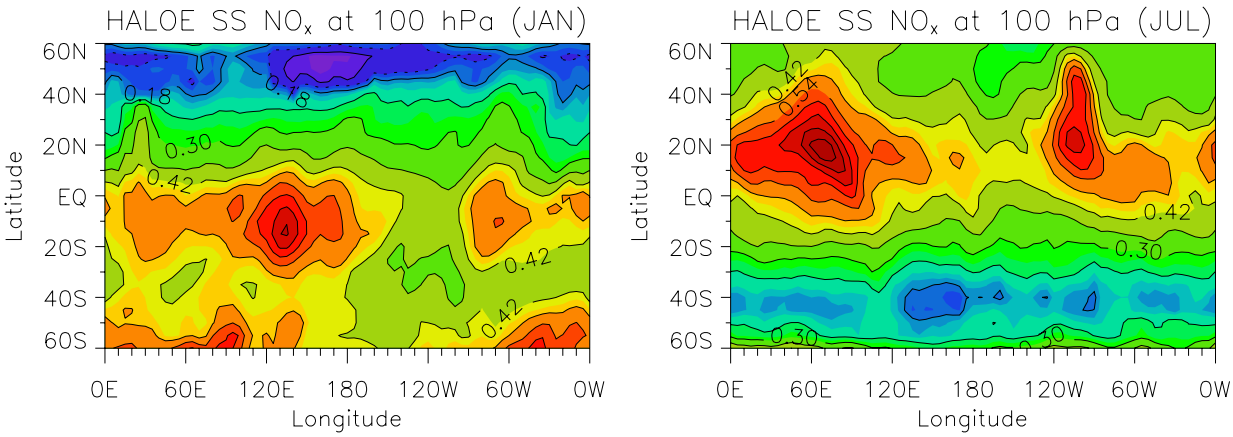

Figure 13. Spatial structure of NO_x (=NO + NO_2) derived from HALOE sunset observations for statistics during January (left) and July (right).

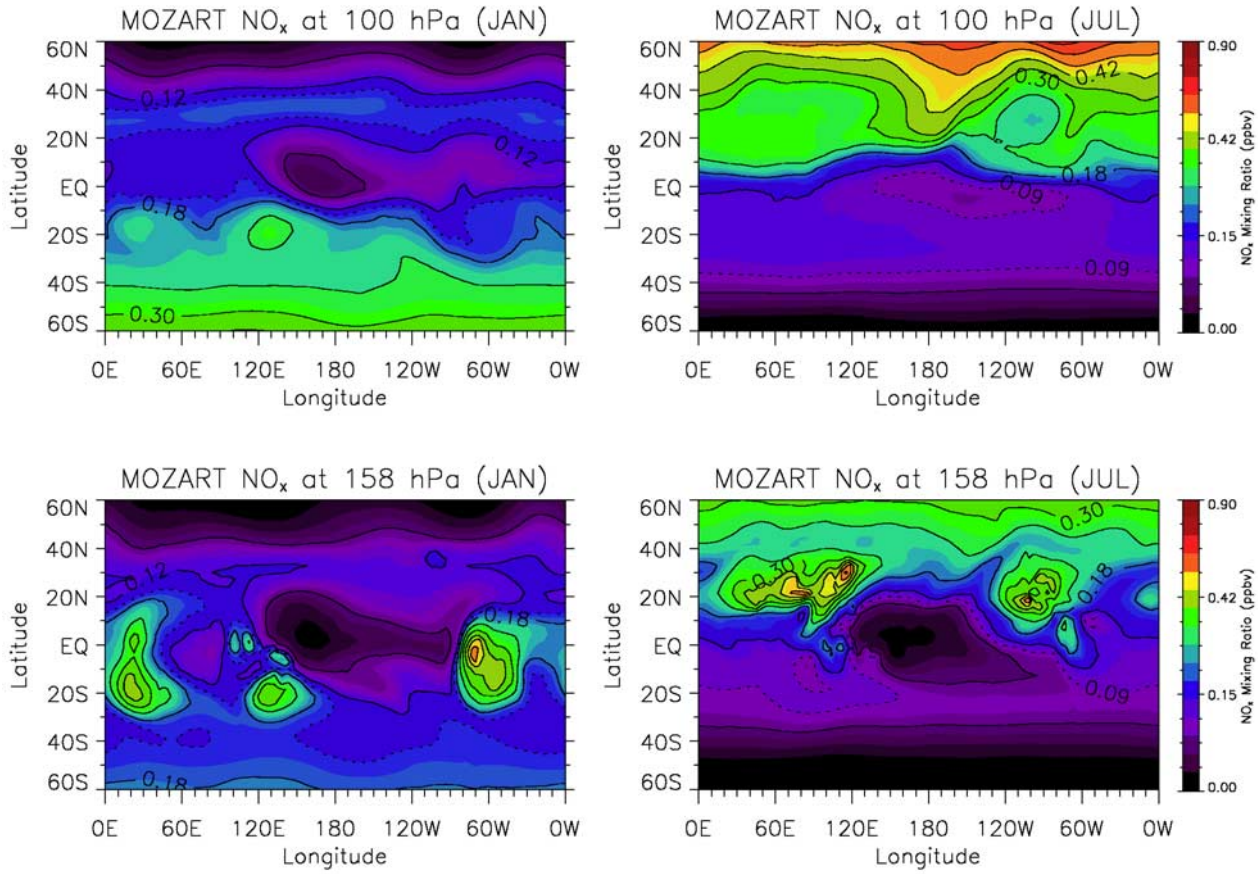

Figure 14. Spatial structure of NO_x derived from the (diurnally averaged) MOZART simulation, showing results at 100 hPa (top) and 158 hPa (bottom), for January (left) and July (right).

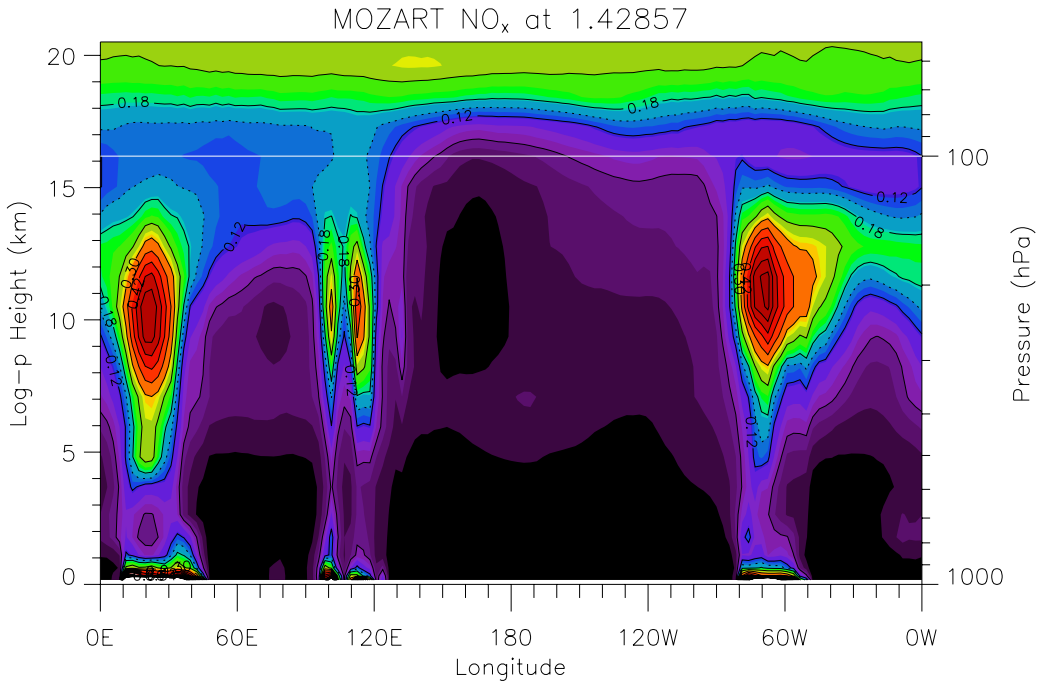

Figure 15. Height-longitude section of MOZART NO_x at the equator in January.

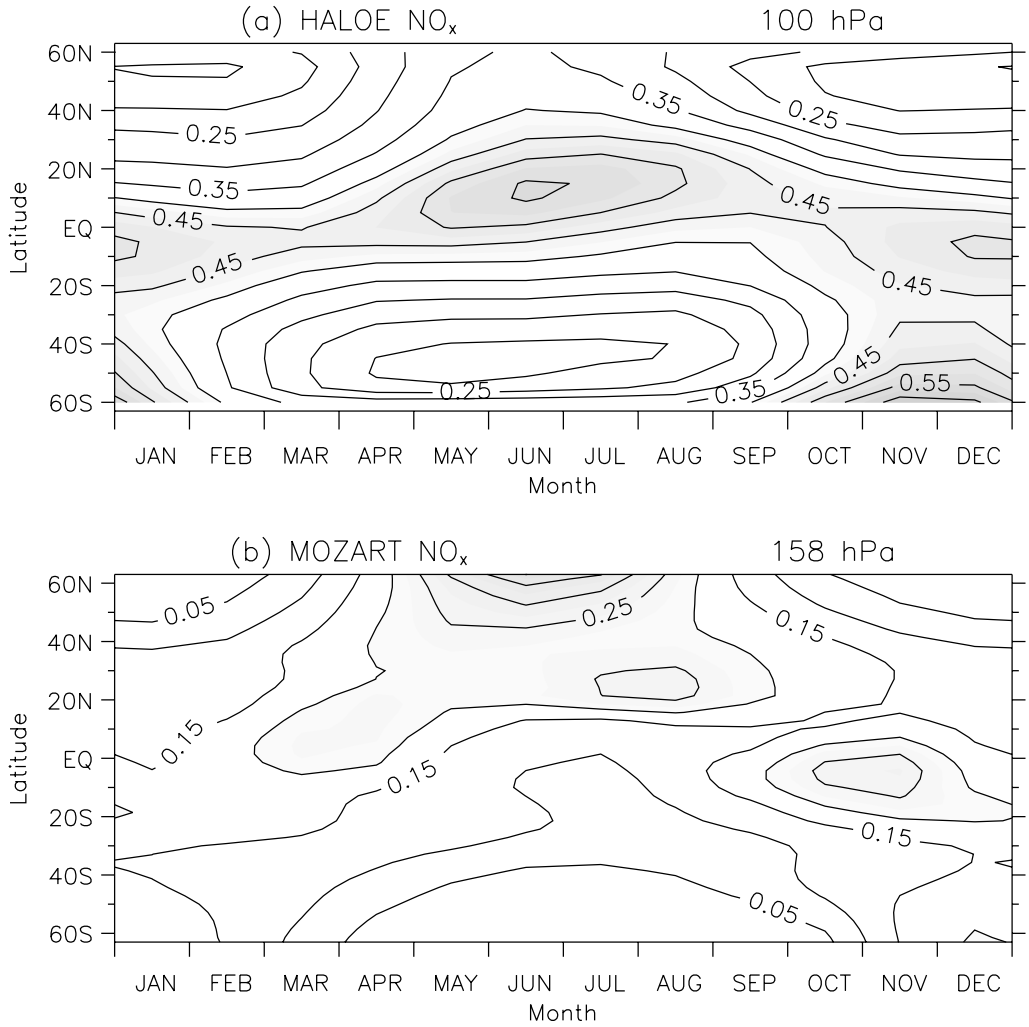

Figure 16. Latitude-time sections of zonally averaged NO_x from (a) 100 hPa HALOE sunset observations and (b) 158 hPa MOZART diurnal average simulation. Contour interval is 0.05 ppbv.

ences between them. At 158 hPa, MOZART exhibits NO_x maxima over low latitude continental regions with magnitudes ~0.3–0.4 ppmv (related to lightning generated NO_x, as discussed below). These maxima are absent in MOZART at 100 hPa. The spatial patterns in HALOE 100 hPa data (Figure 13) agree better with the MOZART 158 hPa results, although the HALOE values are approximately twice as large, and cover larger geographical areas. The MOZART results at 100 hPa show relative minima (NO_x "holes") in the tropics (especially clear in January), which is completely different from the HALOE maxima.

[33] The cause of the tropical NO_x "holes" minima at 100 hPa in the MOZART simulation can be understood from Figure 15, showing which shows a zonal section of MOZART calculated NO_x at the equator over 0–20 km. Three upper-tropospheric NO_x maxima are observed in association with convection over land (Africa, Indonesia, and South America). These maxima are due to parameterized production of NO_x by lightning in convection [see, e.g., *Hauglustaine et al.*, 2001], and reach up to 158 hPa, but not to 100 hPa (see also Figure 14). Model convection in the tropics is also present to the east of Indonesia (~140–200°E), but at these longitudes there is a minimum in upper troposphere NO_x due to vertical transport of near-surface air, which is poor in NO_x. The difference in behavior between continental and oceanic convective regions arises because the model lightning parameterization generates NO_x preferentially over land (where lightning is most intense); over the oceans, the effect of transport from the clean, marine boundary layer (where air NO_x is low) dominates. The upper tropospheric NO_x minimum over the western and central Pacific Ocean extends upward to slightly above 100 hPa, and this explains the minima in calculated NO_x in the tropics seen in Figure 15.

[34] Figure 16 compares latitude-time sections of zonal average NO_x between the HALOE 100 hPa sunset observations and the 158 hPa (diurnal average) MOZART simulation. HALOE exhibits maxima in the tropics, with peaks in the summer subtropics (which mimics tropical convection). MOZART shows a qualitatively similar behavior at 158 hPa, but the maxima are much weaker, and the seasonal peaks occur at different times (note the maximum in October–November). The MOZART results at 100 hPa (not shown) reveal a tropical minimum throughout the year, very different from HALOE. Both HALOE and MOZART results at 100 hPa show seasonal maxima over high lati-

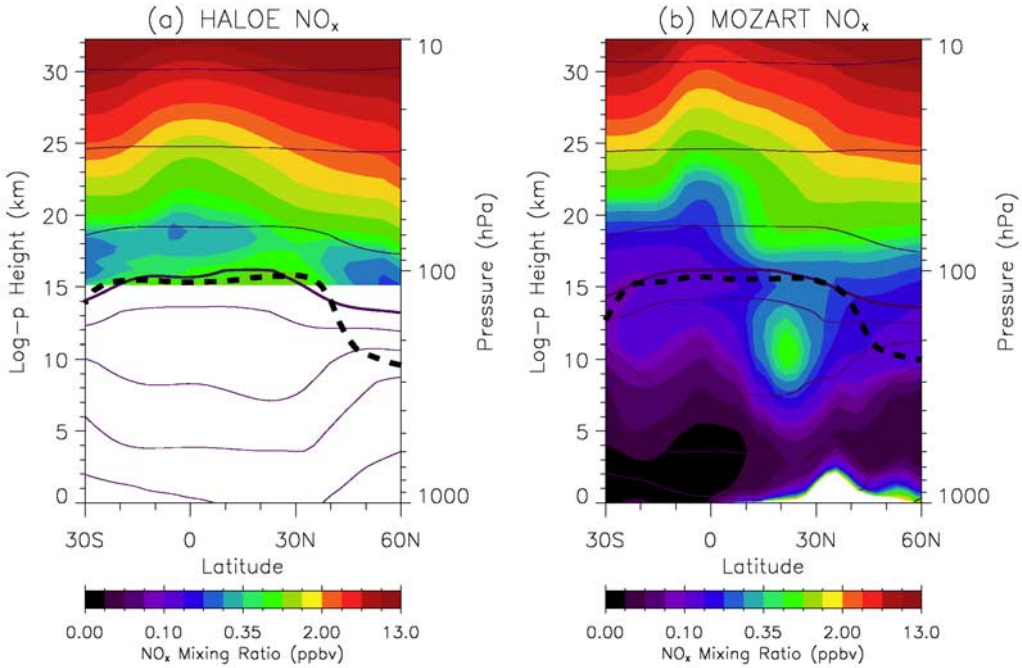

Figure 17. Meridional cross sections of NO_x in the South Asian monsoon region (40°–100°E) in September, derived from (a) HALOE data and (b) MOZART simulation.

tudes of both hemispheres (with peaks over summer polar regions), but the MOZART 100 hPa maxima are almost twice as large as those in the HALOE data.

[35] It is interesting to further compare the HALOE and MOZART NO_x structure near the South Asian monsoon maximum in July (Figures 13–14). Figure 17 shows cross sections through this region in September for both HALOE and MOZART. The MOZART results show an upper tropospheric NO_x maximum (summertime convection over land), which extends across the tropopause into the lower stratosphere (similar to the CH_4 and H_2O results shown in Figures 5 and 10). Although we have not calculated an NO_x budget, Figure 17 implies that the upper tropospheric NO_x produced by (parameterized) lightning contributes to the lower stratosphere maximum observed over this region. While the HALOE observations do not extend into the troposphere, the HALOE data in Figure 17 show a clear maximum in the monsoon region near and above the tropopause, similar to the MOZART result. These similar HALOE patterns suggest that some tropospheric NO_x may enter the stratosphere directly in this region, as occurs in the model.

4. Summary and Discussion

[36] Overall, the MOZART simulations of CH_4 and H_2O in the tropopause region compare favorably with the HALOE observations, in terms of seasonality and global variability. The simulation of UTLS water vapor in particular places stringent constraints on a model in terms of temperature and transport characteristics, and the realistic tape recorder and global variability in MOZART (Figures 6 and 8) are encouraging. An outstanding issue is that the wet phase of the MOZART seasonal cycle in the lower stratosphere is too moist (e.g., Figure 6). This is not simply due to warm temperature biases in the model, and because of the complex interplay of dehydration and transport, no simple cause has been identified.

[37] The seasonal comparisons shown here highlight the importance of the NH summer monsoon circulations for contributing to STE, as discussed in *Dethof et al.* [1999]. In particular, the CH_4 and H_2O fields in both HALOE and MOZART show the localized impact of the South Asian monsoon in the tropopause region, and the MOZART cross sections (Figures 5, 10, and 11) suggest direct transport of constituents into the lower stratosphere via monsoon circulations. Among other things, this transport accounts for the large inter-hemispheric asymmetry in lower stratospheric H_2O (e.g., Figure 8). Furthermore, the MOZART simulations suggest that the relatively moist monsoon air is transported equatorward, and contributes to the "wet" phase of the tropical tape recorder (Figure 11), although little evidence of this is seen in HALOE observations. Quantification of the NH summer monsoon contribution to STE (in comparison to transport in the deep tropics, entrained into the upward Brewer-Dobson circulation) is a challenging topic for future work. Also, the detailed mechanisms of such exchange have only recently received attention [*Dethof et al.*, 1999; *Popovic and Plumb*, 2001].

[38] Relatively large differences are found between the HALOE NO_x observations near the tropopause (100 hPa) and MOZART simulations. There are substantial uncertainties associated with the HALOE NO_x data near 100 hPa, due to relatively weaker signals, retrieval uncertainties and the vertical resolution of ~2 km. However, there are few other observational data sets for NO_x in this altitude region for comparison. Aircraft measurements of NO_x associated with lightning, e.g., *Ridley et al.* [1996], and *Hauglustaine*

et al. [2001], typically extend to only 10–12 km altitude. The NO_y climatology of *Strahan* [1999] (derived from ER-2 measurements) show values in the deep tropics over theta levels 370–400 K of ~0.3–0.5 ppbv, which is in reasonable agreement with the HALOE sunset NOx estimates here. However, the ER-2 climatology is based on very limited data in the tropics, with the available measurements sampled only over the central Pacific ocean, well away from the maxima over convection suggested by the HALOE data. The HALOE NO_x values of order 0.5–0.8 ppbv near 100 hPa (~16 km) are consistent with the lightning simulations of *Pickering et al.* [1998], in particular for conditions of tropical continental convection. Overall the climatological NOx patterns derived from HALOE data seem reasonable, but the exact magnitudes and fine details should be treated cautiously.

[39] Much of the HALOE-MOZART NO_x differences near the tropopause appear related to the vertical extent of lightning generation and convective transport of NO_x in the model: the lightning parameterization generates maxima in the upper troposphere (over land), but these do not extend strongly to tropopause level (Figures 14 and 15). Additionally, the MOZART simulations produce relative NO_x minima over oceanic convection, due to convective transport of low, near surface NO_x (the parameterization of lightning NO_x in MOZART is triggered mainly for convection over land). In spite of the uncertainties associated with HALOE NO_x data, the comparisons here suggest these local minima are unrealistic, and suggest the need for further scrutiny of the NO_x lightning parameterization for the UTLS region.

[40] The HALOE data suggest that NO_x may be a useful tracer for studying stratosphere-troposphere interactions, due to localized sources (resulting in strong gradients) and long lifetimes. The MOZART results show a clear NO_x maximum above the South Asian monsoon, extending into the lower stratosphere (Figure 17), which is suggestive of a lightning NO_x source transported upward via the monsoon circulation.

[41] **Acknowledgments.** This research was partially supported by the Climate Environment System Research Center and the BK 21 program of the Korean Government. We acknowledge support from the NASA ACMAP program, and thank two anonymous reviewers for their constructive comments and suggestions. NCAR is sponsored by the U.S. National Science Foundation.

References

Andrews, A. E., K. A. Boering, B. C. Daube, S. C. Wofsy, E. J. Hintsa, E. M. Weinstock, and T. P. Bui (1999), Empirical age spectra for the lower tropical stratosphere from in situ observations of CO_2: Implications for stratospheric transport, *J. Geophys. Res.*, *104*, 26,581–26,595.

Beaver, G. M., and J. M. Russell III (1998), The climatology of stratospheric HCl and HF observed by HALOE, *Adv. Space Res.*, *21*, 1373–1382.

Boering, K. A., et al. (1995), Measurements of stratospheric carbon dioxide and water vapor at northern midlatitudes: Implications for troposphere-to-stratosphere transport, *Geophys. Res. Lett.*, *22*, 2737–2740.

Boville, B. A. (1995), Middle atmosphere version of CCM2 (MACCM2), Annual cycle and interannual variability, *J. Geophys. Res.*, *100*, 9017–9039.

Brasseur, G. P., J.-F. Müller, and D. Granier (1996), Atmospheric impact of NO_x emission by subsonic aircraft: A three-dimensional model study, *J. Geophys. Res.*, *101*, 1423–1428.

Brasseur, G. P., D. A. Hauglustaine, S. Walters, P. J. Rasch, J.-F. Muller, C. Granier, and X. X. Tie (1998), MOZART: A global chemical transport model for ozone and related chemical tracers: 1. Model description, *J. Geophys. Res.*, *103*, 28,265–28,289.

Brühl, C., P. J. Crutzen, and J.-U. Grooß (1998), High-latitude, summertime NO_x activation and seasonal ozone decline in the lower stratosphere: Model calculations based on observations by HALOE on UARS, *J. Geophys. Res.*, *103*, 3587–3597.

Crutzen, P. J. (1970), The influence of nitrogen oxides on the atmospheric ozone content, *Q. J. R. Meteorol. Soc.*, *96*, 320–327.

Dethof, A., A. O'Neill, J. M. Slingo, and H. G. J. Smit (1999), A mechanism for moistening the lower stratosphere involving the Asian summer monsoon, *Q. J. R. Meteorol. Soc.*, *125*, 1079–1106.

Dlugokencky, E. J., K. A. Masarie, P. M. Lang, and P. P. Tans (1998), Continuing decline in the growth rate of the atmospheric methane burden, *Nature*, *393*, 447–450.

Dlugokencky, E. J., K. A. Masarie, P. M. Lang, P. P. Tans, L. P. Steele, and E. G. Nisbet (1994), A dramatic decrease in the growth rate of atmospheric methane in the northern hemisphere during 1992, *Geophys. Res. Lett.*, *21*, 45–48.

Friedl, R. (Ed.) (1997), Atmospheric effects of subsonic aircraft: Interim assessment report of the advanced subsonic technology program, *NASA Ref. Publ.*, *1400*, 143 pp.

Garcia, R. R., and S. Solomon (1994), A new numerical model of the middle atmosphere: 2. Ozone and related species, *J. Geophys. Res.*, *99*, 12,937–12,951.

Gordley, L. L., et al. (1996), Validation of nitric oxide and nitrogen dioxide measurements made by the Halogen Occultation Experiment for UARS platform, *J. Geophys. Res.*, *101*, 10,241–10,266.

Hall, T. M., D. W. Waugh, K. A. Boering, and R. A. Plumb (1999), Evaluation of transport in atmospheric models, *J. Geophys. Res.*, *104*, 18,815–18,839.

Harries, J. E., J. M. Russell III, A. F. Tuck, L. L. Gordley, P. Purcell, K. Stone, R. M. Bevilacqua, M. Gunson, G. Nedoluha, and W. A. Traub (1996), Validation of measurements of water vapor from the Halogen Occultation Experiment (HALOE), *J. Geophys. Res.*, *101*, 10,205–10,216.

Hauglustaine, D. A., G. P. Brasseur, S. Walters, P. J. Rasch, J.-F. Müller, L. K. Emmons, and M. A. Carroll (1998), MOZART: 2. Model results and evaluation, *J. Geophys. Res.*, *103*, 28,291–28,335.

Hauglustaine, D., L. Emmons, M. Newchurch, G. Brasseur, T. Takao, K. Matsubara, J. Johnson, B. Ridley, J. Stith, and J. Dye (2001), On the role of lightning NO_x in the formation of tropospheric ozone plumes: A global model perspective, *J. Atmos. Chem.*, *38*, 277–294.

Hervig, M. E., J. M. Russell III, L. L. Gordley, J. Daniels, S. R. Drayson, and J. H. Park (1995), Aerosol effects and corrections in the Halogen Occultation Experiment, *J. Geophys. Res.*, *100*, 1067–1079.

Hintsa, E. J., E. M. Weinstock, A. E. Dessler, J. G. Anderson, M. Loewenstein, and J. R. Podolske (1994), SPADE H_2O measurements and the seasonal cycle of stratospheric water vapor [H_2O], *Geophys. Res. Lett.*, *21*, 2559–2562.

Holton, J. R., and W. Choi (1988), Transport circulation deduced from SAMS trace species data, *J. Atmos. Sci.*, *45*, 1929–1939.

Holton, J. R., P. H. Haynes, M. E. McIntyre, A. R. Douglas, R. B. Rood, and L. Pfister (1995), Stratosphere-troposphere exchange, *Rev. Geophys*, *33*, 403–439.

Horowitz, L. W., S. Walters, D. L. Mauzerall, L. K. Emmons, P. J. Rasch, C. Granier, X. Tie, J-F. Lamarque, M. Schultz, and G. P. Brasseur (2004), A global simulation of tropospheric ozone and related tracers: Description and evaluation of MOZART, version 2, *J. Geophys. Res.*, doi:10.1029/2002JD002853, in press.

Houghton, J. T., L. G. M. Filho, B. A. Gallander, N. Harries, A. Kattenberg, and K. Maskell (Eds.) (1996), *Climate Change 1995: The Science of Climate Change*, 567 pp., Cambridge Univ. Press, New York.

Houghton, J. T., Y. Ding, D. J. Griggs, M. Noguer, P. J. van der Linden, and D. Xiaosu (Eds.) (2001), *Climate Change 2001: The Scientific Basis*, 944 pp., Cambridge Univ. Press, New York.

Intergovernmental Panel on Climate Change (2001), *Climate Change 2001: The Scientific Basis*, 881 pp., Cambridge University Press, New York.

Jackson, D. R., S. J. Driscoll, E. J. Highwood, J. E. Harries, and J. M. Russell III (1998), Troposphere to stratosphere transport at low latitudes as studied using HALOE observations of water vapour 1992–1997, *Q. J. R. Meteorol. Soc.*, *124*, 169–192.

Jones, R. L., and J. A. Pyle (1984), Observations of CH_4 and N_2O by the NIMBUS 7 SAMS: A comparison with in situ data and two dimensional numerical model calculations, *J. Geophys. Res.*, *89*, 5263–5279.

Kalnay, E., et al. (1996), The NCEP/NCAR 40-year reanalysis project, *Bull. Am. Meteorol. Soc.*, *77*, 437–471.

Kiehl, J. T., J. J. Hack, G. B. Bonan, B. A. Boville, D. L. Williamson, and P. J. Rasch (1998), The National Center for Atmospheric Research community climate model: CCM3, *J. Clim.*, *11*, 1131–1149.

Lin, S. J., and R. B. Rood (1996), A fast flux form semi-Lagrangian transport scheme on the sphere, *Mon. Weather Rev.*, *124*, 2046–2070.

McCormick, M. P., E. W. Chiou, L. R. McMaster, W. P. Chu, J. C. Larsen, D. Rind, and S. Oltmans (1993), Annual variations of water vapor in the stratosphere and upper troposphere observed by the Stratospheric Aerosol and Gas Experiment II, *J. Geophys. Res.*, *98*, 4867–4874.

Mote, P. W., K. H. Rosenlof, M. E. McIntyre, E. S. Carr, J. C. Gille, J. R. Holton, J. S. Kinnersley, H. C. Pumphrey, J. M. Russell III, and J. W. Waters (1996), An atmospheric tape recorder: The imprint of tropical tropopause temperatures on stratospheric water vapor, *J. Geophys. Res.*, *101*, 3989–4006.

Newell, R. E., and S. Gould-Stewart (1981), A stratospheric fountain?, *J. Atmos. Sci.*, *38*, 2789–2796.

Park, J. H., et al. (1996), Validation of Halogen Occultation Experiment CH_4 measurements from the UARS, *J. Geophys. Res.*, *101*, 10,813–10,203.

Pickering, K. E., Y. Wang, W.-K. Tao, C. Price, and J.-F. Müller (1998), Vertical distributions of lightning NO_x for use in regional and global chemical transport models, *J. Geophys. Res.*, *103*, 31,203–31,216.

Popovic, J. M., and R. A. Plumb (2001), Eddy shedding from the upper-tropospheric Asian monsoon anticyclone, *J. Atmos. Sci.*, *58*, 93–104.

Price, C., J. Penner, and M. Prather (1997), NO_x from lightning: 1. Global distribution based on lightning physics, *J. Geophys. Res.*, *102*, 5929–5941.

Randel, W. J., F. Wu, J. M. Russell III, A. Roche, and J. Waters (1998), Seasonal cycles and QBO variations in stratospheric CH_4 and H_2O observed in UARS HALOE data, *J. Atmos. Sci.*, *55*, 163–185.

Randel, W. J., F. Wu, A. Gettelman, J. M. Russell III, J. M. Jawodny, and S. J. Oltmans (2001), Seasonal variation of water vapor in the lower stratosphere observed in Halogen Occultation Experiment data, *J. Geophys. Res.*, *106*, 14,313–14,325.

Rasch, P. J., and J. E. Kristjansson (1998), A comparison of the CCM3 model climate using diagnosed and predicted condensate parameterizations, *J. Clim.*, *11*, 1587–1614.

Ridley, B. A., J. Dye, J. Walega, J. Zheng, F. Grahek, and W. Rison (1996), On the production of active nitrogen by thunderstorms over New Mexico, *J. Geophys. Res.*, *101*, 20,985–21,005.

Rosenlof, K. H., A. F. Tuck, K. K. Kelly, J. M. Russell III, and M. P. McCormick (1997), Hemispheric asymmetries in water vapor and inferences about transport in the lower stratosphere, *J. Geophys. Res.*, *102*, 13,213–13,234.

Russell, J. M., III, L. L. Gordley, J. H. Park, S. R. Drayson, W. D. Hesketh, R. J. Cicerone, A. F. Tuck, J. E. Frederick, J. E. Harries, and P. J. Crutzen (1993), The Halogen Occultation Experiment, *J. Geophys. Res.*, *98*, 10,777–10,797.

Schoeberl, M. R., M. Luo, and J. E. Rosenfield (1995), An analysis of the Antarctic Halogen Occultation Experiment trace gas observations, *J. Geophys. Res.*, *100*, 5159–5172.

Schroeder, W. J., and M. S. Shepherd (1988), Geometry-based fully automatic mesh generation and the Delaunay triangulation, *Int. J. Numer. Methods Eng.*, *26*, 2503–2515.

Seinfeld, J. H., and S. N. Pandis (1998), *Atmospheric Chemistry and Physics: From Air Pollution to Climate Change*, 1326 pp., John Wiley, Hoboken, N. J.

Simpson, I. J., D. R. Blake, F. S. Roland, and T.-Y. Chen (2002), Implications of the recent fluctuations in the growth rate of tropospheric methane, *Geophys. Res. Lett.*, *29*(10), 1479, doi:10.1029/2001GL014521.

Strahan, S. E. (1999), Climatologies of lower stratospheric NO_y and O_3 and correlations with N_2O based on in situ observations, *J. Geophys. Res.*, *104*, 30,463–30,480.

Stratospheric Processes and Their Role in Climate (SPARC) (1999), *SPARC Assessment of Upper Tropospheric and Stratospheric Water Vapour*, edited by D. Kley, J. M. Russell III, and C. Phillips, *SPARC Rep.. 2*, *WCRP Rep.113*, *WMO/TD Rep.1043*.

SPARC (2002), *SPARC Intercomparison of Middle Atmosphere Climatologies*, edited by W. Randel, M. L. Chanin, and C. Michaut, *SPARC Rep. 3*., Paris.

Williamson, D. L., and J. G. Olson (1994), Climate simulation with a semi-Lagrangian version of the NCAR Community Climate Model, *Mon. Weather Rev.*, *117*, 102–129.

Zhang, R., N. T. Sanger, R. E. Orville, X. Tie, W. Randel, and E. R. Williams (2000), Enhanced NO_x by lightning in the upper troposphere and lower stratosphere inferred from the UARS global NO_2 measurements, *Geophys. Res. Lett.*, *27*, 685–688.

W. Choi and M. Park, School of Earth and Environmental Sciences, Seoul National University, Gwanak-gu, Seoul, 151-747, Korea. (wchoi@snu.ac.kr; marcia@strat.snu.ac.kr)

R. R. Garcia, D. E. Kinnison, and W. J. Randel, National Center for Atmospheric Research, 1850 Table Mesa Drive, Boulder, CO 80305, USA. (rgarcia@ucar.edu; dkin@ucar.edu; randel@ucar.edu)